21st International Conference on
Harmonisation within Atmospheric Dispersion Modelling for Regulatory Purposes
27-30 September 2022, Aveiro, Portugal

INNOVATIVE PROBABILISTIC MODELLING OF RISK ZONES IN THE EVENT OF ACCIDENTAL ATMOSPHERIC RELEASES

Maéva Caillat[1], Valentin Pibernus[1], Sylvain Girard[1], Patrick Armand[2] and Christophe Duchenne[2]

[1]PHIMECA Engineering, F-75012 Paris, France
[2]CEA, DAM, DIF, F-91297 Arpajon, France

Abstract: 3D models present very promising prospects for simulating the local-scale and high-resolution distribution of releases which are potentially dangerous for human health and the environment. To encourage the taking into account of their results by the rescue teams and their authorities, it is today very desirable that the concentration or dose maps produced by the 3D models also provide information on the uncertainties associated with them. To do so, we developed a methodology to accurately estimate the probability of exceeding a concentration threshold in the event of accidental or malevolent releases into the atmosphere. This methodology assesses uncertainty with confidence or credible intervals using alternatively the frequentist approach and a novel Bayesian approach based on spatial Gaussian processes able to lower the limit of significance of the probability estimation. The Bayesian approach was validated on synthetic data, then used in the frame of a real situation inspired by the Lubrizol accident in January 2013 in Rouen (France). We show that the Bayesian model gives more accurate and narrower than the classical confidence intervals, and is able to lower the significance limit of the estimate, thus to draw decision maps which are of real help in view of decision-making.

Key words: *Atmospheric dispersion, danger zones, uncertainty estimation, probabilistic approach.*

INTRODUCTION

At the local scale, the flow and dispersion in the atmosphere are strongly influenced not only by the synoptic meteorological situation, but also by the details of topography and land-use and the presence of buildings, if any. Thus, 3D models are well suited for the assessment of chemical or radiological releases into the air that may have consequences on human health and the environment. These models are more and more used both for regulatory purposes and emergency preparedness and response. Decision-makers, like operators of industrial facilities, civil security officials or public authorities, would be ready to exploit these models provided they are embedded in operational decision-support systems. Moreover, the scientific community and, increasingly, the users are well aware of the uncertainties on the input data of the models, the models themselves and the representativeness of their results. It is therefore highly desirable that part of the research on atmospheric dispersion be oriented towards taking uncertainties into account.

In this short paper, we take an interest in a case study inspired by the industrial accident that occurred in January 2013, at the Lubrizol chemical plant located in Rouen (France). Operational mistakes and system failures in the plant resulted in extended releases of hydrogen sulfide and mercaptan, both of which are foul-smelling when they exceed a specified concentration. The features of the incident are very complex in several respects, namely the terrain characterized by a rugged topography and alternating industrialized, urban and natural areas, the long-lasting and variable kinetics of the releases combined with the highly fluctuating meteorological conditions during and after the releases.

We simulated the dispersion of pollutants in the atmosphere using a modeling system whose input data, notably meteorological or related to the source term, are extremely uncertain. While epistemic uncertainties are not the only ones, taking them into account in a probabilistic framework is absolutely required for reliable decision-making (Girard *et al.*, 2020). In this study, our objective was to estimate the probability of exceeding a concentration threshold that might represent a certain level of danger in the context of atmospheric dispersion. We took a step-by-step approach. We estimated the area where the concentration threshold was exceedeed by a unique deterministic simulation. Then, we performed several simulations and evaluated point by point the probability of exceedance of the concentration threshold. Then, we tried to

estimate the confidence and credible intervals associated to a given probability of exceedance. While this approach succeeds in accounting for the uncertainties, it highlights the limit of significance. Eventually, to lower this limit, we used a credible interval with a conditional spatial independence criterion.

In the short paper, we present the PMSS simulations carried out to create the Lubrizol accident data set, the deterministic map of the area where a given concentration threshold is exceeded, the probabilistic decision map of the same area and the confidence intervals, our Bayesian approach exploiting the spatial correlation of the concentrations, and finally, the results of this approach, which are commented on.

PMSS FLOW AND DISPERSION SIMULATIONS

The simulations were performed with Parallel-Micro-SWIFT-SPRAY (PMSS). Originally, Micro-SWIFT-SPRAY (MSS) (Tinarelli *et al.* ,2013) was developed to provide a simplified but rigorous CFD solution in a limited amount of time of the flow and dispersion in built-up environments. MSS combined the high resolution local scale versions of SWIFT and SPRAY models. SWIFT is a 3D diagnostic mass-consistent model using a terrain-following vertical coordinate. Large-scale meteorological data, local meteorological measurements, and analytical results of formulae in building-modified flow areas, if any, are interpolated and adjusted to generate 3D wind fields. Turbulent flow parameters are also computed by SWIFT to be used by SPRAY. SPRAY is a Lagrangian particle dispersion model able to take into account the presence of obstacles. The dispersion of the release is simulated by following the trajectories of a large number of numerical particles. Trajectories are obtained by integrating in time the particle velocity, which is the sum of a transport component defined by the local averaged wind, generally provided by SWIFT and a stochastic component, representing the dispersion due to atmospheric turbulence.

SWIFT and SPRAY handle complex terrains and changing meteorological conditions, as well as specific release features, such as heavy or light gases. Recently, SWIFT and SPRAY were parallelized across time, space and numerical particles, resulting in the PMSS system (Oldrini *et al.*, 2017). The parallelism was shown to be very efficient, both on a multi-core laptop and on clusters of several hundreds of cores in a high-performance computing center (Oldrini *et al.*, 2019) (Armand *et al.*, 2021). PMSS was systematically validated against experimental wind tunnel and field campaigns for short and extended releases (Trini Castelli *et al.*, 2018). In all configurations, the PMSS results complied with the statistical acceptance criteria defined by Hanna and Chang (2012) used for validating dispersion models in built-up environments.

DETERMINISTIC DECISION MAP

We simulated chemical concentrations in the air generated by the accident that happened on January 2013 at the Lubrizol chemical plant in Rouen (France). Hydrogen sulfide and mercaptan were released from the plant stacks throughout the accident. Consequently, thousands of people smelled the chemicals, some of them suffering from nausea and headaches. In our study, we considered the 35-kilometer wide square area centered on the incident site. The simulation covered a 35-hour period, so that all hazardous materials were either deposited or left the simulation domain by the end of the period. The input meteorological data were obtained from the community weather reconstruction and forecast meso-scale modelling system WRF (Skamarock *et al.*, 2005). The source term was adapted from data established by Ismert and Durif (2014). Our objective was to predict whether an arbitrary concentration threshold was exceeded on the studied area over the whole period. We chose a threshold value, namely 2 $\mu g.cm^{-3}$, to create a fictitious restricted area where the population and first responders could be at risk. **Figure 1** shows the results of the deterministic simulation. Even if this model enables us to make some predictions on the concentrations, it does not take account of uncertainty. Yet, the inputs are substantially uncertain, and the results are too.

PROBABILISTIC DECISION MAP AND CONFIDENCE INTERVALS

Next, we accounted for uncertainty in the input parameters and carried out 100 simulations using PMSS with different sets of the wind speed, wind direction, rain intensity, and release rate of the chemical. The small sample size is representative of an emergency, for which results must be given as quickly as possible, while each simulation requires up to one hour and are run in parallel on suitable computing resources.

Let $Y(s,t)$ be the term of propagation of uncertainty, *i.e.* the chemical concentration at a given point s and time t. In the study, we focus on the maximum temporal concentration at each location throughout the simulation $Y(s) = \sup_{t\in[t_0,t_{simu}]} Y(s,t)$. Let $X(s,t)$ be the random vector of uncertainties, which can contain any kind of information, such as the spatial coordinates or distance to the source term or variables like wind speed, wind direction, rain intensity or release rate. Denoting the atmospheric dispersion model by f, we wish to assess the distribution of $Y(s,t) = f\big(X(s,t)\big)$. Let $\zeta \in \mathbb{R}^+$ be a concentration threshold and $Z(s) = I_{\{Y(s)>\zeta\}}$ a variable worth 1 if the concentration exceeds the concentration threshold at a s and 0 otherwise. $p_X(s) = \Pr(Y(s) > \zeta)$ represents the probability that the concentration at s is higher than the concentration threshold. Z follows a Bernoulli distribution of parameter p_X: $Z \sim \mathcal{B}(p)$. Let $p_{lim} \in \mathbb{R}^+$ be the threshold of the probability of exceeding a concentration. We focus on the event $\{p_X(s) > p_{lim}\}$ to make decision.

Let's now consider independent and identically distributed random variables $Z_i(s)$ $\{i = 0 \dots n\}$ that follow a Bernoulli distribution of parameter $p_X(s)$. Let $S_n(s) = \sum_{i=1}^{n} Z_i\,(s) \sim \mathcal{B}\big(n, p_X(s)\big)$ be the number of times the concentration at s exceeds the threshold or the binomial distribution with parameters n and $p_X(s)$. In a previous work (Girard *et al.*, 2020), we estimated $p_X(s)$ with the sample mean estimator $\hat{P}_n(s) = S_n/n$. **Figure 2** shows the estimated probabilities of exceeding the chosen threshold concentration of 2 µg.cm^{-3}. Colors indicate the probability from 0 (yellow) to 1 (black).

Unfortunately, a decision based on a point estimator does not inform us about the estimation uncertainty, contrary to credible and confidence intervals (*N.B.* credible intervals account for an actual observed sample, here dispersion simulations, which is not the case for confidence intervals). These intervals set limits to $p_X(s)$ thanks to two estimators, the lower and upper bounds of the interval $L_X(S_n(s),\alpha)$ and $U_X(S_n(s),\alpha)$. Let $I_X(n,s,\alpha)$ be a confidence or credible interval which contains $p_X(s)$ with a confidence level of $1-\alpha$, with α the risk accepted to be as low as possible. The actual coverage probability at a fixed value of p_X is an estimate of the probability that the interval actually contains p_X. A conservative interval has its actual coverage probability greater or equal to the nominal confidence level $1-\alpha$. Conversely, a mean correct interval has a mean coverage probability of at least $1-\alpha$, but its actual coverage probability is lower for extreme values of p_X, close to 0 or 1. In this study, we focused on mean correct intervals, as they are narrower than conservative ones. For $n \geq 40$, Brown *et al.* (2001) recommend the adjusted Wald interval, also called Add 4 (Agresti and Coull, 1998). A confidence or credible interval is divided into three zones, each one with a different decision-making. **Figure 3** shows examples of these maps:

- In the red area where the lower bound of the interval is greater than p_{lim}, there is strong evidence that we exceed the critical level at location s.
- In the white area where the upper bound of the interval is lower than p_{lim}, there is strong evidence that we are below the critical level at location s.
- In the grey area where p_{lim} is enclosed by the interval bounds, it is not easy to compare p_X and p_{lim} and the result is non significant.

The left and right decision maps on **Figure 3** are computed with the same data and parameters, except for the probability threshold p_{lim}. It illustrates the loss of significativity phenomenon: when p_{lim} goes under a certain value (dependent on sample size and confidence level), the map becomes useless to the decider!

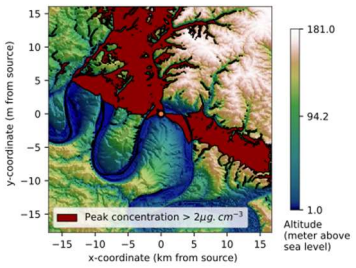

Figure 1. Concentration map of the chemical with a given concentration threshold.

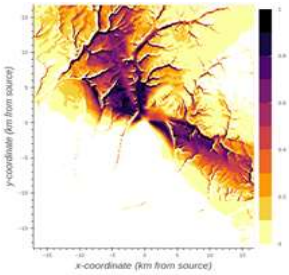

Figure 2. Probability of exceeding the concentration threshold with the sample mean.

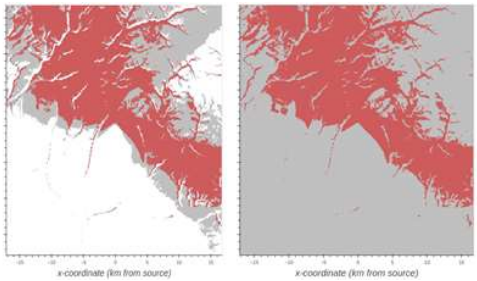

Figure 3. Decision maps accounting for credible intervals computed with the same parameters, except for the probability threshold p_{lim} going from 5% (left) to 4% (right).

INTRODUCING SPATIAL CORRELATION IN THE BAYESIAN APPROACH

In the previous model, the n-sample $Z_1(s),\dots,Z_n(s)$ of $Z(s)$ was supposed to be independent for every location $s \in \mathbb{R}^2$ and the spatial structure of the data was ignored. However, any geostatistical data have a continuously varying response in space. Therefore, the information in location s may help improving the estimations in nearby points $s+h$. From now on, let's consider Bayesian statistics, where the parameter p_X becomes the random variable P_X, and the hierarchical model inspired from Diggle and Ribeiro (2007):

$$S_n(s) \mid P_X(s) = \sum_{i=1}^{n} Z_i(s) \mid P_X(s) \sim \mathcal{B}\big(n, p_X(s)\big) \quad (1)$$

$$logit\big(P_X(s)\big) \mid \beta, \tau, \lambda \sim \text{GaussianProcess}\left(X^T(s)\,\beta, \gamma(h) = \tau\, exp\left(-\frac{\|h\|}{\lambda}\right)\right) \quad (2)$$

with $X(s)$ the design matrix, β a mean parameter, τ a variance parameter, and λ a scale parameter. Equation (1) assumes the conditional independence of $S_n(s)$ which is the number of times the concentration threshold is exceeded at location s. A spatial Gaussian process $\{SGP(s): s \in \mathbb{R}^2\}$ is a stochastic process of which the joint distribution $SGP = \{SGP(s_1) \dots SGP(s_K)\}$ is multivariate normal for every set of positions $\{s_1 \dots s_K\}$ with $s_j \in \mathbb{R}^2$. Any such process is completely defined by its mean function $\mu(s) = \mathbb{E}[SGP(s)]$, and its covariance function $\gamma(s, s') = \text{cov}\big(SGP(s), SGP(s')\big)$.

For a set of positions $\{s_1 \dots s_K\}$, let's define the isotropic spatial Gaussian process SGP_X as this:

$$SGP_X = \{SGP_X(s_1) \dots SGP_X(s_K)\} = \big\{logit\big(P_X(s_1)\big) \dots logit\big(P_X(s_K)\big)\big\} \sim \mathcal{N}_K(\mu, \Sigma) \quad (3)$$

with the K-dimensional mean vector $\mu = \big(\mu(s_j)\big)_{j=1}^{K} = \big(X^T(s_j)\beta\big)_{j=1}^{K} = X^T\beta$,

and the KxK-dimensional matrix Σ such that $\Sigma_{ij} = \gamma(s_i, s_j) = \tau exp\left(-\frac{\|s_i - s_j\|}{\lambda}\right)$.

The covariance function $\gamma: \mathbb{R}^2 \times \mathbb{R}^2 \to [0, \tau]$ is negligible with respect to τ at a distance of more than 3λ.
The design matrix is $X(s) = [1 \quad X^{(1)}(s) \quad X^{(2)}(s) \quad X^{(3)}(s)]^T$ with the explanatory variables being $X^{(1)}(s)$ the y-coordinate, $X^{(2)}(s)$ the x-coordinate, and $X^{(3)}(s)$ the distance to the source term.

Prior distributions encode our initial knowledge about the parameters of the model. As the parameters $(\beta_i)_{i \in [\![1,4]\!]}$ can take any value in $\mathbb{R}$, we choose a normal distribution *a priori*: $\forall i \in [\![1,4]\!]\ \beta_i \sim \mathcal{N}\big(\mu_{\beta_i}, \sigma^2_{\beta_i}\big)$. As the parameter τ is the variance of $SGP_X(s)$ for any location, we choose an inverse gamma distribution because it is defined on $\mathbb{R}^+$ and induces conjugate distributions: $\tau \sim \text{InvGamma}(\delta_\tau, \phi_\tau)$. As the parameter λ must be strictly positive, we choose a gamma distribution a priori: $\lambda \sim \Gamma(k_\lambda, \theta_\lambda)$.

To build the posterior distribution of $\{P(s_j): j \in [\![1,K]\!]\}$ from n observations of $Z(s_j)$, we use Monte Carlo Markov chains whose stationary distribution corresponds to the posterior distribution in Bayesian statistics. Except for τ which is an inverse gamma distribution, the posterior distributions of β_i, λ and $SGP_X(s_j)$ are constructed using the Metropolis-Hastings algorithm within a Gibbs sampler (Geman and Geman, 1984). Finally, we built a Markov chain for β, τ, λ and $SGP_X(s_j)$, that is to say a chain of dimension $lenbeta$ (the dimension of β) + 2 + K (the number of points of the map).

RESULTS OF THE BAYESIAN APPROACH AND DISCUSSION

Application and validation of the spatial Gaussian process

First, the method was tested on simulated data to ensure the existence of the parameters β^{true}, τ^{true} and λ^{true}, which we tried to retrieve. We generated a simulation SGP_X^{simu} of the spatial Gaussian process $SGP_X \sim \mathcal{N}\big(X^T\beta^{true}, \Sigma(\tau^{true}, \lambda^{true})\big)$. SGP_X is a vector of dimension K, which we can represent as an exceedance probability map of dimension $\sqrt{K} \times \sqrt{K}$ by applying to it the expit function which sends $\mathbb{R}$ to [0,1]. Thus, we used this realization to simulate $S_n^{\text{simu}}(s) \sim \mathcal{B}(n, P_X^{\text{simu}}(s) = expit\left(SGP_X^{\text{simu}}(s)\right)$.

We assigned fictive values to the parameters ($\beta^{true} = [-8, 0.2, 0.2, -0.3]$, $\tau^{true} = 1$, $\lambda^{true} = 1$, and $n = 100$) to assess the model and considered uninformative or low-informative prior distributions as follows:

$\forall i \in [\![1,4]\!]\ \beta_i \sim \mathcal{N}\big(\mu_{\beta_i} = 0, \sigma^2_{\beta_i} = 100\big)$, $\tau \sim \text{InvGamma}(\delta_\tau = 1, \phi_\tau = 1)$, and $\lambda \sim \Gamma(k_\lambda = 2, \theta_\lambda = 0.5)$

Figure 4 shows a realization of this process used as the target for the probability estimation algorithm.

In the next step, β_i were randomly initialized between -1 and 1. We arbitrarily initialized τ at 1 because it is the order of magnitude of the parameters that interest us: $\tau \leq 0.1$ is almost trivial and $\tau \geq 10$ renders very unstructured, white noise type maps. We also arbitrarily initialized λ at 1 so that it adapts to the size of the map. Expert knowledge could allow a better initialization on real data. Since we suspect that the true value of S is around the sample mean, we initiliazed $SGP_X(s_j)$ at its sample mean. We fixed the variances of the proposal kernels to have an acceptance rate close to 0.234.

Markov chains (not presented in this short paper) of the MCMC algorithm were output for 10,000 iterations, removing the first 2,000 terms, notably the burning period, as well as one term out of two to reduce the temporal dependence of the chain. The MCMC algorithm has good mixing properties, since the output Markov chains look like a Gaussian noise. All the chains are centered on their true parameters: $\beta_{mean} = [-7.95, 0.20, 0.21, -0.31]$, $\tau_{mean} = 1.06$, and $\lambda_{mean} = 1.03$. As expected, τ and λ are highly correlated.

Performances of the Bayesian method

While the Bayesian approach slightly improves point estimation, its main interest lies in interval estimation. To compare the Bayesian and Add 4 intervals, we generated 1,000 maps of size 10 x 10, thus a total of 100,000 different locations and we drew $n = 100$ realizations of $\mathcal{B}(P(s))$. From this sample, we estimated the uncertainty on $P_X(s)$ by building Bayesian and Add 4 credible intervals for each location. We could then compute the average coverage probability by assessing how many intervals contained the actual value $P_X(s)$ among the 100,000 different locations. **Table 1** compares the performances of the Bayesian and Add 4 intervals, computed with the test case illustrated in **Figure 4**. With smaller average coverage probability, Bayesian intervals are slightly less conservative, but they achieve significantly smaller expected widths (20% on average) than those computed with the Add 4 method, which make them an attractive choice.

Table 1. Average coverage probability and expected width of the Bayesian and the Add 4 intervals.

Interval	Average coverage probability	Expected width
Bayesian at 95%	94.3% ± (8.2% x 10^{-2})	(1.29 x 10^{-1}) ± (5.9 x 10^{-4})
Bayesian at 99%	98.3% ± (4.4% x 10^{-2})	(1.64 x 10^{-1}) ± (7.5 x 10^{-4})
Add 4 at 95%	95.6% ± (6.6% x 10^{-2})	(1.55 x 10^{-1}) ± (5.0 x 10^{-4})
Add 4 at 99%	99.2% ± (2.9% x 10^{-2})	(2.04 x 10^{-1}) ± (6.6 x 10^{-4})

Bayesian intervals as part of a decision making process

Bayesian intervals bring two improvements when drawing decision maps as those on **Figure 3**:

- It reduces the width of the gray zone of a significant amount.
- It counteracts the loss of significativity by preventing the grey zone to spread when considering small probability threshold or small risk, what is the main interest of our Bayesian estimator.

Figure 5 shows the decision maps drawn with the Add 4 confidence interval and our Bayesian hierarchical model for the Lubrizol data set. It illustrates the capacity of the Bayesian estimator to be robust against loss of significativity and produce a map that, unlike the Add 4 interval, is actually usable by decision-makers.

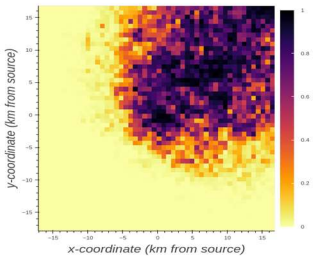

Figure 4. Target probability map generated for testing the Bayesian algorithm.

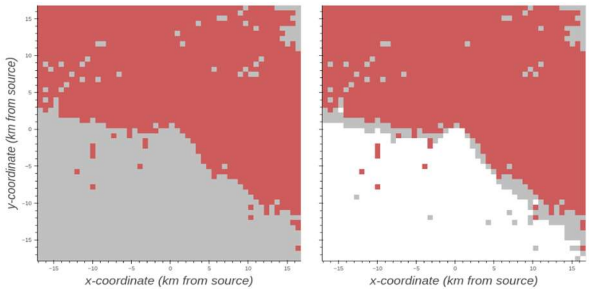

Figure 5. Decision maps obtained with the Add4 interval (left) and the Bayesian estimators (right).

Computational times

Computational times on an Intel Core i7-10810U processor with a speed between 1.1 GHz and 4.9 GHz are given in **Table 2** for different numbers of locations *K* and 10,000 MCMC iterations. The MCMC algorithm is very time-consuming and the main limitation in the implementation of the Bayesian hierarchical model in comparison with the Add 4 method.

Table 2. Computational time depending on the number of locations K and for $N_{chain} = 10,000$ iterations.

Number of locations	MCMC computation time	Add 4 computation time
25	9 s	0.01 s
900	28 min 7 s	0.11 s
2,500	12 h 48 min 1 s	0.22 s

CONCLUSION

In this short paper, we compare two different strategies for building decision maps from interval estimation of the probability of exceeding a concentration threshold: the classical frequentist approach and a novel Bayesian approach. This is a step forward decision maps built-up from point estimation of the exceedance probabilities presented in Girard *et al.* (2020). The Bayesian approach is extensively tested with synthetic data and applied to a case study inspired by the Lubrizol accident in January 2013 in Rouen (France).

While confidence or credible intervals are associated with a controllable nominal risk and extremely useful to construct decision maps, they have a limit of significance. Indeed, when the sample size, the accepted risk and/or the probability threshold become small, the decision map may be of no use to make decisions. To solve this problem, we implemented a Bayesian hierarchical model based on spatial Gaussian processes to encode the spatial dependence of the probabilities of exceeding a concentration threshold between nearby points in the probabilistic model. We showed on simulated data that the Bayesian model was more accurate and narrower than the Add 4 confidence intervals, and able to lower the significance limit of the estimate, thus to draw informative decision maps when Add 4 was of no help for this. However, the computational time of the Bayesian model was much longer than Add 4, especially for a large number of points on maps.

To the best of our knowledge, this is the first time that a scientifically reliable method has the potential to provide information in emergency involving atmospheric releases on the confidence level of concentration maps. In the future, we plan to reduce the computational time of the Bayesian model by running iterations of the MCMC algorithm simultaneously and making points absolutely independent after a certain distance. We also plan to transform our decision method into an interactive and user-friendly tool that could help better grasp the concept of estimation uncertainty on decision maps.

REFERENCES

Agresti, A. and B.A. Coull, 1998: Approximate is better than "exact" for interval estimation of binomial proportions. The American Statistician, 52 (2), 119–126.

Armand, P., O. Oldrini, C. Duchenne and S. Perdriel, 2021: Topical 3D modelling and simulation of air dispersion hazards as a new paradigm to support emergency preparedness and response. Environmental Modelling & Software, 143, 105–129.

Brown, T.T., L.D.Cai and A. Das Gupta, 2001: Interval estimation for a binomial proportion. Statistical Science, 16 (2), 101–117.

Geman, S. and D. Geman, 1984: Stochastic relaxation, Gibbs distributions, and the Bayesian restoration of images. IEEE PAMI-6.

Girard, S., P. Armand, C. Duchenne and T. Yalamas, 2020: Stochastic perturbations and dimension reduction for modelling uncertainty of atmospheric dispersion simulations. *Atmospheric Environment*, 117313.

Hanna, S. and J. Chang, 2012: Acceptance criteria for urban dispersion model evaluation. Meteorology and Atmospheric Physics, 116, 133–146.

Ismert, M. and M. Durif. 2014: Accident de Lubrizol du 21 janvier 2013. Couplage entre dispersion du nuage odorant et plaintes et appréciation des risques sanitaires associés. Rapport INERIS-DRC-13-137709-03375 B.

Oldrini, O., P. Armand, C. Duchenne and S. Perdriel., 2019: Parallelization performances of PMSS flow and dispersion modelling system over a huge urban area. *Atmosphere*, 10 (7), 404–420.

Oldrini, O., P. Armand, C. Duchenne, C. Olry, J. Moussafir and G. Tinarelli, 2017: Description and preliminary validation of the PMSS fast response parallel atmospheric flow and dispersion solver in complex built-up areas. *Environmental Fluid Mechanics*, 17 (5), 997–1014.

Tinarelli, G., L. Mortarini, S. Trini Castelli, G. Carlino, J. Moussafir, C. Olry, P. Armand and D. Anfossi, 2013: Description and preliminary validation of the PMSS fast response parallel atmospheric flow and dispersion Solver in complex built-up areas, American Geophysical Union (AGU), No. 200 (A), 311–327.

Skamarock, W.C., J.B. Klemp, J. Dudhia, D.O. Gill, D.M. Barker, W. Wang and J.G. Powers, 2005: A description of the advanced research WRF version 2. National Center For Atmospheric Research, Boulder (CO), USA.

Trini Castelli, S., P. Armand, G. Tinarelli, C. Duchenne and M. Nibart, 2018: Validation of a Lagrangian particle dispersion model with wind tunnel and field experiments in urban environment. Atmospheric Environment, 193, 273–289.